Pergamon

Acta mater. 49 (2001) 463–472

Acta MATERIALIA

www.elsevier.com/locate/actamat

SOLUTE SEGREGATION AND COHERENT NUCLEATION AND GROWTH NEAR A DISLOCATION—A PHASE-FIELD MODEL INTEGRATING DEFECT AND PHASE MICROSTRUCTURES

S. Y. HU and L. Q. CHEN*

Department of Materials Science and Engineering, The Pennsylvania State University, University Park, PA 16802, USA

(Received 24 July 2000; received in revised form 15 September 2000; accepted 21 September 2000)

Abstract—A diffuse-interface field model is proposed for describing diffusional processes in coherent systems with arbitrary microstructures and arbitrary spatial distribution of structural defects such as dislocations. It takes into account the effect of both the coherency elastic energy of a microstructure and the elastic coupling between the coherency strains and defect strains. In this model, any arbitrary spatial distribution of defects is described using the micromechanics concept of space-dependent "stress-free" or "eigen" strains. As examples, the solute segregation as well as the nucleation and diffusional growth of a coherent precipitate around an edge dislocation are considered. It is shown that coherent nucleation may become barrierless under the influence of the local elastic field of a dislocation.

Keywords: Nucleation, growth; Segregation; Diffuse-interface; Microstructure

1. INTRODUCTION

Many important processes in crystalline solids, such as diffusional phase transformations and microstructure coarsening, involve diffusional redistribution of atoms under the influence of stresses [1–3]. The stresses may arise from, for example, a composition-dependent lattice parameter, an external field, or the presence of internal structural defects. Recent theoretical and modeling studies have been mainly focused on the effect of coherency stresses due to a composition-dependent lattice parameter (see for example [4–13]) and for a rather thorough list of references on this subject, see a recent review [14]. Coherent compositional stresses are shown to have significant or sometimes dominating effects on mesoscale microstructure morphologies and the kinetics of their evolution [14].

It has long been recognized that structural defects such as dislocations also play an important role in diffusional processes and phase transformations in solids. For example, the interaction between composition and a dislocation results in solute segregation and depletion, leading to the formation of so-called "Cottrell atmosphere" [15]. The nucleation of a second-phase precipitate at a dislocation was first considered by Cahn who assumed that a cylindrical nucleus replaces the dislocation core, thus providing additional driving force for nucleation compared to that in the bulk [16]. The elastic energy of the solid solution and the coherency strain energy of the precipitate itself were ignored. Dollins [17] and Barnett [18] considered the nucleation of a coherent precipitate in the presence of an edge dislocation. For coherent nucleation, the additional driving force for nucleation results from the interactions between the stress field of the dislocation and that of the coherent precipitate. In order to obtain analytical solutions for the elastic strain energy, the elastic property of the solid solution is assumed to be isotropic and only the dilatational stress-free strain for the precipitate was considered. In addition, the compositional inhomogeneity induced by the dislocation field is ignored in calculating the elastic strain energy. Xiao and Hassen [19] re-examined the coherent nucleation problem near an edge dislocation by considering the effect of Cottrell atmosphere on coherent nucleation. However, they again had to assume isotropic elastic modulus for the solid solution and a spherical shape for the nucleus. More recently, the effect of structural defects on nucleation during structural phase transitions was investigated using a Landau-type of static thermodynamic approach [20].

To relax many of the assumptions in the analytical

* To whom all correspondence should be addressed. Tel.: +1-814-863-8101; fax: +1-814-865-0016.
E-mail address: chen@ems.psu.edu (L.Q. Chen)

1359-6454/01/$20.00
PII: S1359-6454(00)00331-1

theories and to study the actual kinetic diffusional processes, there have been a number of computer simulation models proposed for studying the interactions between defects and phases. For example, Wang *et al.* studied the segregation profile around an edge dislocation, and the effect of segregation on dislocation dynamics using a discrete Monte-Carlo model [21]. The interactions between dislocations and coherent precipitates were studied by Lee using the discrete atom method (DAM) [22] and Voorhees [23] by solving the diffusion equation in the presence of a dislocation. The effect of dislocations on the morphological evolution during spinodal decomposition was investigated by Léonard and Desai who directly introduced the analytical elastic solution of a dislocation [24] into the Cahn–Hilliard equation [25].

In this work, we propose a continuum diffuse-interface field model by coupling the Cahn–Hilliard diffusion equation [25] with the elastic fields produced from coherent compositional inhomogeneities as well as from structural defects such as dislocations, grain boundaries, cracks, inclusions, etc. This model can easily incorporate elastic anisotropy and allows arbitrary distribution of composition and defects. The unique feature of this model is that the elastic fields from structural defects and coherent compositional inhomogeneity are obtained within exactly the same formulation using the concept of "eigenstrains" in micromechanics. As a result, not only the coupling between the elastic fields of a composition and those of a defect, but also the elastic interactions among the defects are automatically taken into account. This feature will become particularly convenient when the dynamics of defects such as dislocation motion are considered in the future. Furthermore, since analytical solutions for the elastic fields of defects are not required, any complicated defect configurations can be modeled. This is different from the approach of Léonard and Desai, which requires the analytical solution for the dislocation field [24] and the interactions among dislocations were ignored.

In the following sections, we will first extend the elastic energy calculation [1] for coherent microstructures to systems with both a compositional inhomogeneity and structural defects. In Section 2, we will present the Cahn–Hilliard diffusion equation incorporating both the compositional coherency stress and the stresses due to structure defects. In Section 3, we will first discuss the numerical calculation of the stress-field around a dislocation and compare to analytical expressions. We will then show two examples for applying the Cahn–Hilliard diffusion equation with both coherent compositional and defect stresses. The first example is the classical problem involving solute segregation around an edge dislocation. In the second example, we will demonstrate that a coherent nucleus may be stabilized by the local elastic field of a dislocation. Although our model is formulated for three dimensions, for simplicity, we perform all the simulations in two dimensions. Furthermore, the homogeneous modulus approximation is adopted.

2. ELASTIC ENERGY OF A COHERENT COMPOSITION INHOMOGENEITY WITH STRUCTURAL DEFECTS

We consider a simple binary solid solution with a compositional inhomogeneity described by $X(\mathbf{r})$, representing the mole or atom fraction X at position $\mathbf{r}$. If we assume that the variation of stress-free lattice parameter, a, with composition obeys Vegard's law, the local stress-free strain caused by compositional inhomogeneity is given by

$$\epsilon^{\mathrm{o}}_{ij}(\mathbf{r}) = \epsilon_{\mathrm{o}}\delta X(\mathbf{r})\delta_{ij} \tag{1}$$

where $\epsilon_{\mathrm{o}} = 1/a\ \mathrm{d}a/\mathrm{d}X$ is the composition expansion coefficient of lattice parameter, $\delta X(\mathbf{r}) = X(\mathbf{r}) - X_{\mathrm{o}}$ with X_{o} being the overall composition of the solid solution, and δ_{ij} is the Kronecker-delta function.

For structure defects such as point defects, dislocations, twin and grain boundaries, cracks, and inhomogeneous inclusions, their spatial distributions can also be described by stress-free strains or eigenstrains, $\epsilon^{\mathrm{d}}_{ij}(\mathbf{r})$ [26].

Let us use $\epsilon_{ij}(\mathbf{r})$ to denote the total strain measured with respect to the homogeneous solution with composition X_{o}, then Hook's law gives the local elastic stress,

$$\sigma^{\mathrm{el}}_{ij}(\mathbf{r}) = \lambda_{ijkl}[\epsilon_{kl}(\mathbf{r}) - \epsilon^{\mathrm{o}}_{kl}(\mathbf{r}) - \epsilon^{\mathrm{d}}_{kl}(\mathbf{r})] \tag{2}$$

where λ_{ijkl} are the elastic constants.

Since the mechanical equilibrium with respect to elastic displacements is established much faster than any diffusional processes, for any given distribution of composition, the system is always at mechanical equilibrium,

$$\frac{\partial \sigma^{\mathrm{el}}_{ij}}{\partial r_j} = 0 \tag{3}$$

where r_j is the jth component of the position vector, $\mathbf{r}$. Following Khachaturyan [1], the total strain $\epsilon_{ij}(\mathbf{r})$ may be represented as the sum of homogeneous and heterogeneous strains:

$$\epsilon_{ij}(\mathbf{r}) = \bar{\epsilon}_{ij} + \delta\epsilon_{ij}(\mathbf{r}) \tag{4}$$

where the homogeneous strain, $\bar{\epsilon}_{ij}$, is defined so that

$$\int_{\mathrm{V}} \delta\epsilon_{ij}(\mathbf{r})\mathrm{d}^3 r = 0 \tag{5}$$

The homogeneous strain is the uniform macroscopic strain characterizing the macroscopic shape and volume change associated with the total strain, $\epsilon_{ij}(\mathbf{r})$. Let us use $u_i(\mathbf{r})$ to denote the ith component of the displacement. The heterogeneous strain and its corresponding displacements are related through

$$\delta\epsilon_{kl}(\mathbf{r}) = \frac{1}{2}\left[\frac{\partial u_k(\mathbf{r})}{\partial r_l} + \frac{\partial u_l(\mathbf{r})}{\partial r_k}\right] \tag{6}$$

Substituting equations (2), (4) and (6) into the mechanical equilibrium equation (3), and assuming that the elastic constants are homogeneous, one has

$$\lambda_{ijkl}\frac{\partial^2 u_k}{\partial r_j \partial r_l} = \lambda_{ijkl}\left[\epsilon_o\delta_{kl}\frac{\partial \delta X}{\partial r_j} + \frac{\partial \epsilon^d_{kl}}{\partial r_j}\right] \tag{7}$$

Solving the above equation in Fourier space, we have

$$u_k(\mathbf{g}) = -\mathrm{i}G_{ik}(\mathbf{g})[\sigma^o_{ij}\delta X(\mathbf{g}) + \sigma^d_{ij}(\mathbf{g})]g_j \tag{8}$$

where $\mathbf{g}$ is the wave vector, g_i is the ith component of $\mathbf{g}$, $\mathrm{i} = \sqrt{-1}$, $u_k(\mathbf{g})$ and $\delta X(\mathbf{g})$ are the Fourier transforms of $u_k(\mathbf{r})$ and $\delta X(\mathbf{r})$, $G_{ik}(\mathbf{g})$ is the inverse tensor to $(G^{-1}(\mathbf{g}))_{ik} = g^2\lambda_{ijkl}n_jn_l = g^2\Omega^{-1}_{ik}(\mathbf{n})$ with $\mathbf{n} = \mathbf{g}/|g|$, $\sigma^o_{ij} = \lambda_{ijkl}\epsilon_o\delta_{kl}$, $\sigma^d_{ij}(\mathbf{g}) = \lambda_{ijkl}\epsilon^d_{kl}(\mathbf{g})$, and $\epsilon^d_{kl}(\mathbf{g})$ is the Fourier transform of $\epsilon^d_{kl}(\mathbf{r})$. The corresponding heterogeneous strain $\delta\epsilon_{ij}(\mathbf{r})$ in Fourier space is given by

$$\delta\epsilon_{ij}(\mathbf{g}) = \frac{\mathrm{i}}{2}[u_i(\mathbf{g})g_j + u_j(\mathbf{g})g_i] \tag{9}$$

The total elastic energy of a system containing coherent compositional inhomogeneities described by $\delta X(\mathbf{r})$, and structural defects described by the eigenstrain distribution, $\epsilon^d_{ij}(\mathbf{r})$, is then given by

$$E = \frac{1}{2}\int_v \lambda_{ijkl}\epsilon^{el}_{ij}(\mathbf{r})\epsilon^{el}_{kl}(\mathbf{r})\mathrm{d}V \tag{10}$$

Substituting the elastic solution [equation (9)] for heterogeneous strain into the above elastic energy expression [equation (10)] and taking into account the fact that $\int_v \delta\epsilon_{ij}(\mathbf{r})\mathrm{d}V = 0$ and $\int_v \delta X(\mathbf{r})\mathrm{d}V = 0$, we have

$$\begin{aligned} E = {} & \frac{V}{2}\lambda_{ijkl}\bar{\epsilon}_{ij}\bar{\epsilon}_{kl} + \frac{V}{2}\lambda_{ijkl}\delta_{ij}\delta_{kl}\epsilon_o^2\overline{[\delta X(\mathbf{r})]^2} \\ & -\frac{1}{2}\int_g \frac{\mathrm{d}^3\mathbf{g}}{(2\pi)^3}n_i\sigma^o_{ij}\Omega_{jk}(\mathbf{n})\sigma^o_{kl}n_l|\delta X(\mathbf{g})|^2 \\ & + \frac{V}{2}\lambda_{ijkl}\overline{\epsilon^d_{ij}(\mathbf{r})\epsilon^d_{kl}(\mathbf{r})} \\ & -\frac{1}{2}\int_g \frac{\mathrm{d}^3\mathbf{g}}{(2\pi)^3}n_i\sigma^d_{ij}(\mathbf{g})\Omega_{jk}(\mathbf{n})\{\sigma^d_{kl}(\mathbf{g})\}^*n_l \\ & -V\lambda_{ijkl}\overline{\bar{\epsilon}_{ij}\epsilon^d_{kl}(\mathbf{r})} + V\sigma^o_{ij}\overline{\delta X(\mathbf{r})\epsilon^d_{ij}(\mathbf{r})} \\ & -\int_g \frac{\mathrm{d}^3\mathbf{g}}{(2\pi)^3}n_i\sigma^o_{ij}\Omega_{jk}(\mathbf{n})\sigma^d_{kl}(\mathbf{g})n_l\delta X^*(\mathbf{g}) \end{aligned} \tag{11}$$

where V is the total volume of the system, $\overline{\ldots}$ represents the average of the quantity … over the entire volume, and $\{\ldots\}^*$ denotes the complex conjugate of $\{\ldots\}$. The total elastic energy given above includes the homogeneous deformation energy of the system (the first term), the total coherency strain energy of a solid solution induced by a compositional inhomogeneity (the second and third terms), the strain energy of a structural defect (fourth and fifth terms), and the interaction energies among the homogeneous deformation, the coherency strain, and the structural defect (the remaining three terms). The homogeneous strain in equation (11) is determined by the boundary constraint. If a boundary is constrained so that the system is not allowed to have any homogeneous deformation, the homogeneous strain, $\bar{\epsilon}_{ij}$, is equal to zero. Similarly, if the system is subject to an initial applied strain, ϵ^a_{ij}, and then the boundary is held fixed, $\bar{\epsilon}_{ij} = \epsilon^a_{ij}$. On the other hand, if the system is stress-free, the homogeneous strain is obtained by minimizing the total elastic energy. In this work, for simplicity, we assume that the boundary is constrained so that $\bar{\epsilon}_{ij} = 0$

3. DIFFUSION EQUATION IN THE PRESENCE OF COMPOSITIONAL STRESS AND DEFECTS

For a binary substitutional solid solution, the diffusion flux is given by

$$J = -N_vM\nabla\mu \tag{12}$$

where N_v is the number of atoms per unit volume, μ is the chemical potential per atom, and M is a mobility given by

$$M = X(1-X)[XM_1 + (1-X)M_2] \tag{13}$$

where M_1 and M_2 are atomic mobilities of species 1 and 2, respectively. They are related to the diffusivity through $M_i = D_i/(k_BT)$ where D_i is the diffusion coefficient of species i in a dilute solution. For simplicity, we assume that the mobilities of the two species are equal, and thus $M = (DX(1-X))/(k_BT)$.

In a compositionally inhomogeneous solid solution with composition-dependent lattice parameter, μ is given by

$$\mu(\mathbf{r}) = \frac{\partial f_{\mathrm{inc}}(X)}{\partial X} - \kappa\nabla^2X + \mu_{\mathrm{el}} \tag{14}$$

where $f_{\text{inc}}(X)$ is the incoherent free energy density of the solid solution, κ is the gradient energy coefficient [27]. In equation (14), $\mu_{\text{el}} = (1/N_v)(\mathrm{d}e_{\text{el}}/\mathrm{d}X)$ is the elastic potential per atom due to the coherency strain and the presence of defects described by $\epsilon^{\text{d}}_{kl}(\mathbf{r})$, and is given by

$$N_v\mu_{\text{el}} = \epsilon_o^2\lambda_{ijkl}\delta_{ij}\delta_{kl}[X(\mathbf{r})-X_{\text{o}}] - \epsilon_o\lambda_{ijkl}\delta_{ij}\delta\epsilon_{kl}(\mathbf{r}) + \epsilon_o\lambda_{ijkl}\delta_{ij}\epsilon^{\text{d}}_{kl}(\mathbf{r}) \tag{15}$$

where $\delta\epsilon_{kl}(\mathbf{r})$ is given by the inverse Fourier transform of $\delta\epsilon_{kl}(\mathbf{g})$. The time-dependent Cahn–Hilliard diffusion equation is then given by [3, 28]

$$\frac{\mathrm{d}X(\mathbf{r})}{\mathrm{d}t} = \nabla\left[\frac{DX(1-X)}{k_{\text{B}}T}\nabla\left[\frac{\partial f_{\text{inc}}(X)}{\partial X} - \kappa\nabla^2X + \mu_{\text{el}}\right]\right] \tag{16}$$

Although the above variable-coefficient diffusion equation can be efficiently solved using the semi-implicit Fourier-Spectral method [29], to avoid unnecessary discussions on the numerical method, we make a further simplification by assuming that the factor $X(1-X)$ is a constant given by $X_{\text{o}}(1-X_{\text{o}})$ where X_{o} is the overall composition.

Using the dimensionless units, $t^* = (DtX_{\text{o}}(1-X_{\text{o}}))/(\Delta x)^2$, $f^*_{\text{inc}} = f_{\text{inc}}/k_{\text{B}}T$, $\mu^*_{\text{el}} = \mu_{\text{el}}/k_{\text{B}}T$, $\nabla^* = (\Delta x)^2\nabla$, $r^* = r/(\Delta x)$, and $\kappa^* = \kappa/(k_{\text{B}}T(\Delta x)^2)$, we have

$$\frac{\mathrm{d}X}{\mathrm{d}t^*} = (\nabla^*)^2\left[\frac{\mathrm{d}f^*_{\text{inc}}(X)}{\mathrm{d}X} - \kappa^*(\nabla^*)^2X + \mu^*_{\text{el}}\right] \tag{17}$$

Taking a Fourier-transform of both sides of equation (17), we have the temporal evolution of the composition wave amplitude, $X(\mathbf{g})$,

$$\frac{\mathrm{d}X(\mathbf{g}^*)}{\mathrm{d}t^*} = -(g^*)^2\left[\left(\frac{\mathrm{d}f^*_{\text{inc}}(X)}{\mathrm{d}X}\right)_{\mathbf{g}^*} + \kappa^*(g^*)^2X(\mathbf{g}^*) + \mu^*_{\text{el}}(\mathbf{g}^*)\right] \tag{18}$$

where g^* is the magnitude of $\mathbf{g}^*$, $X(\mathbf{g}^*)$ and $\mu_{\text{el}}(\mathbf{g}^*)$ are the Fourier transforms of $X(\mathbf{r}^*)$ and $\mu^*_{\text{el}}(\mathbf{r}^*)$, respectively. The above equation is most efficiently solved using a semi-implicit method [29],

$$X(\mathbf{g}^*,t^* + \Delta t^*) = \frac{X(\mathbf{g}^*,t) - \Delta t^*(g^*)^2\left[\left(\frac{\mathrm{d}f^*_{\text{chem}}(X)}{\mathrm{d}X}\right)_{\mathbf{g}^*} + \mu^*_{\text{el}}(\mathbf{g}^*)\right]}{1 + \Delta t^*\kappa^*(g^*)^4} \tag{19}$$

where Δt^* is the time step for integration. Algorithms with higher order in t are also available [29].

4. INTERACTIONS BETWEEN A COMPOSITION FIELD AND A DISLOCATION

4.1. Elastic field of a dislocation

Since the elastic field of a single dislocation is analytically known, for comparison and validation, we first apply the model discussed in the last section to obtaining the stress field around a single dislocation in the absence of compositional inhomogeneity. We consider an edge dislocation line lying along the [001] direction and passing through the origin with a Burger's vector $\mathbf{b} = (0,b_{\text{o}},0)$. According to [2], the eigenstrain for such a dislocation is given by,

$$\epsilon^{\text{d}}_{22}(\mathbf{r}) = b_{\text{o}}\delta(y)H(x) \tag{20}$$

where $\delta(y)$ is the Dirac delta function and $H(x)$ is the Heaviside step function

$$H(x) = \begin{cases} 1 & x>0 \\ 0 & x<0 \end{cases} \tag{21}$$

Other components of the eigenstrain ϵ^{d}_{ij} are zero. The corresponding Fourier transform of the dislocation eigenstrain in equation (20) is given by

$$\epsilon^{\text{d}}_{22}(\mathbf{g}) = \frac{b_{\text{o}}}{\mathrm{i}g_1V} \tag{22}$$

where V is the system volume. To directly use the eigenstrain in equation (22) in a numerical simulation is problematic since the eigenstrain of equation (20) is defined in the whole continuum space while numerical simulations are usually performed using periodic boundary conditions on a discretized grid. However, if a periodic cell is chosen sufficiently large so that the interactions between the dislocation and its images in the neighboring periodic repeating cells can be neglected, one may use equation (22) in determining the stress-field of a dislocation with periodic boundary conditions. The main problem of directly using equation (22) is the fact that the corresponding stress distributions show significant oscillations [see Fig. 1(b)]. In calculating Fig. 1(b), we placed the dislocation at the center of a computational grid [Fig. 1(a)] with a 512×512 grid. The Burgers vector is $b_{\text{o}} = 0.1$ in units of grid size, Δx. The elastic constants are $C_{11} = 300$, $C_{12} = 100$, and $C_{44} = 100$, all in units of $N_vk_{\text{B}}T$, which provides an isotropic elastic solid with a shear modulus of $\mu = C_{44} = 100$, and a Poisson ratio of 0.25. To get rid of the oscillations in the stress field, we propose to use the following two methods for describing the eigenstrain of a dislocation in a numerical simulation.

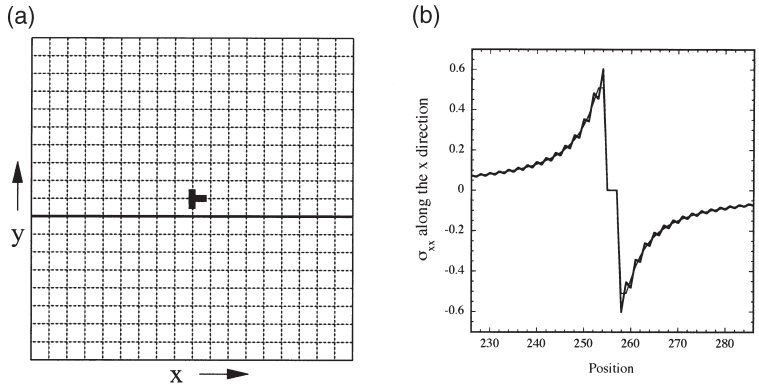

Fig. 1. (a) Schematic illustration of a single dislocation located at the center of a computational grid; (b) local stress σ_{xx} as a function of position along the solid line in (a). Thick line—numerical calculation using eigenstrain [equation (22)]; thin line—analytical solution from continuum elasticity.

One solution to the boundary condition incompatibility is to introduce dislocation loops on discrete lattice points. An example of a dislocation loop in two dimensions is shown in Fig. 2(a). According to the definition in equation (20), the grid points occupied by the dislocation loop with Burgers vector $(0,b_o,0)$ are assigned the following values for the eigenstrain,

$$\epsilon^{d}_{22}(\mathbf{r}) = b_o\theta(\mathbf{r}) \tag{23}$$

where b_o is the magnitude of the Burger's vector and $\theta(\mathbf{r})$ is the shape function depicted in Fig. 2(b). To examine the stress distribution around such a dislocation loop, we considered a system with 1024×1024 grid points. The dislocation loop is placed on a line of grid points between the coordinates (256,512) and (768,512). The elastic constants and the Burgers vector are the same as those for obtaining Fig. 1(b). In this case, $\epsilon^{d}_{22}(\mathbf{g})$ is obtained numerically using Fast Fourier Transforms. The calculated distribution of local pressure, $(\sigma_{xx} + \sigma_{yy})/2$, along the x direction parallel to the dislocation loop but one grip point below [represented by the solid line in Fig. 2(a)] is shown in Fig. 3(a). As one can see, the calculated local pressure values agree well with the corresponding analytical solution represented by open squares and there are no oscillations. However, the xy component of the stress still shows significant oscillations [Fig. 3(b)]. For systems involving only dilatational strains, such as compositional strains discussed below, the dilatational strain only interacts with the local pressure, and the oscillations in the shear component are not very important.

Another way to reduce the oscillations in the dislocation stress field is to describe a dislocation using a spatial distribution of an infinite number of infinitesimal dislocations. In particular, one can use Gaussian functions to describe the Burgers vector distribution of the infinitesimal dislocations,

$$b_i(x,y) = b_{io}\frac{\alpha_1\alpha_2}{\pi}e^{-[\alpha_1^2(x-x_o)^2 + \alpha_2^2(y-y_o)^2]} \tag{24}$$

where (x_o,y_o) is the center of the distribution, α_i $(i = 1,2)$ are coefficients which determine the degree of spatial localization of the dislocation distribution,

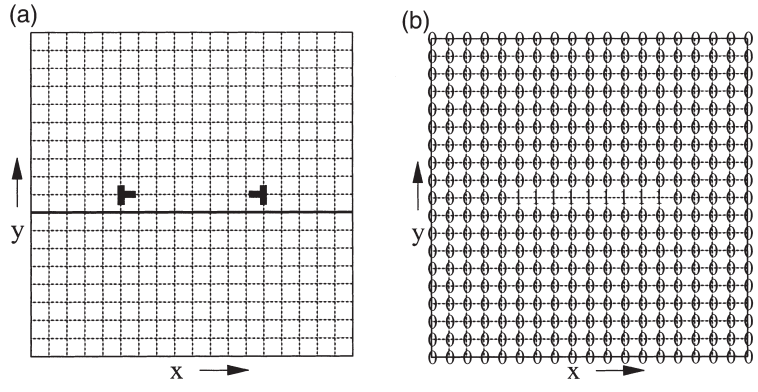

Fig. 2. (a) Schematic representation of a dislocation loop in two dimensions and a discretization grid; (b) the representation of a dislocation loop by the shape function on a discretization grid.

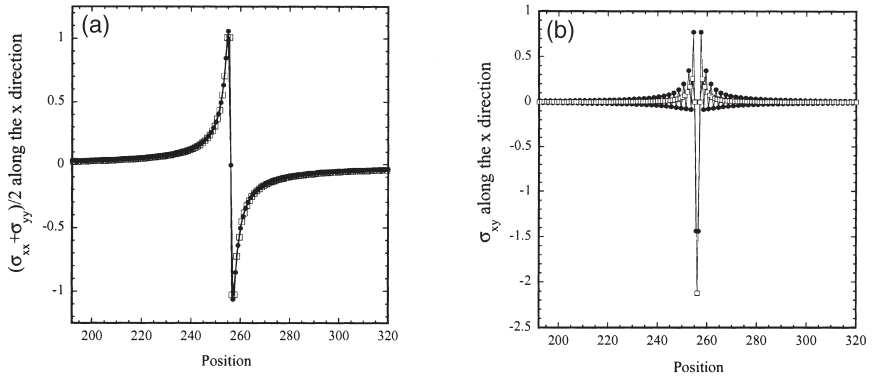

Fig. 3. (a) Local pressure as a function of position along the solid line in Fig. 2(a); (b) shear stress as a function of position along the same line. Solid circles—from the numerical calculation by assigning the eigenstrain on discrete lattice points; open squares—analytical solution from continuum elasticity.

and b_{1o} and b_{2o} are the components of the entire Burgers vector content $\mathbf{b}_o$ of the dislocation. The limiting case, $\alpha_i \to \infty$, corresponds to a dislocation described by a singular δ distribution function as in equation (20). For example, for an edge dislocation with Burgers vector $\mathbf{b} = (0,b_o,0)$ along the z direction, the corresponding eigenstrain tensor can be written as

$$\epsilon^{d}_{22}(x,y) = \frac{b_o\alpha_1\alpha_2}{\pi}\iint e^{-[\alpha_1^2(x_1-x_o)^2 + \alpha_2^2(y_1-y_o)^2]} \delta(y-y_1)H(x-x_1)dx_1dy_1 \quad (25)$$

All other components of the eigenstrain tensor are zero. The corresponding Fourier transform of the above eigenstrain is given by

$$\epsilon^{d}_{22}(g_1,g_2) = \frac{1}{ig_1V} e^{i(g_1x_o + g_2y_o)} e^{-(g_1^2/4\alpha_1^2 + g_2^2/4\alpha_2^2)} \quad (26)$$

With the Gaussian description, the oscillations in the shear components are also essentially eliminated [Fig. 4(a)]. In the calculation, α_1 and α_2 were both set to be 1.0. In Fig. 4(b), we plot the local pressure distribution along the solid line depicted in Fig. 2(a) and compare it with that of an analytical solution using continuum elasticity. The agreement between the Gaussian description and the analytical solutions is very good.

For the following examples, we performed simulations using both of these two methods for introducing the dislocation eigenstrain, equations (23) and (26). The results obtained are very similar, so below we will only present the results obtained using the Gaussian description.

4.2. Solute segregation and Cottrell atmosphere around an edge dislocation

Let us first consider a simple substitutional binary system in which the coherent chemical thermodynamics is described by the ideal free energy of mixing

$$f^*(X) = \frac{f}{k_BT} = X\ln X + (1-X)\ln(1-X) \quad (27)$$

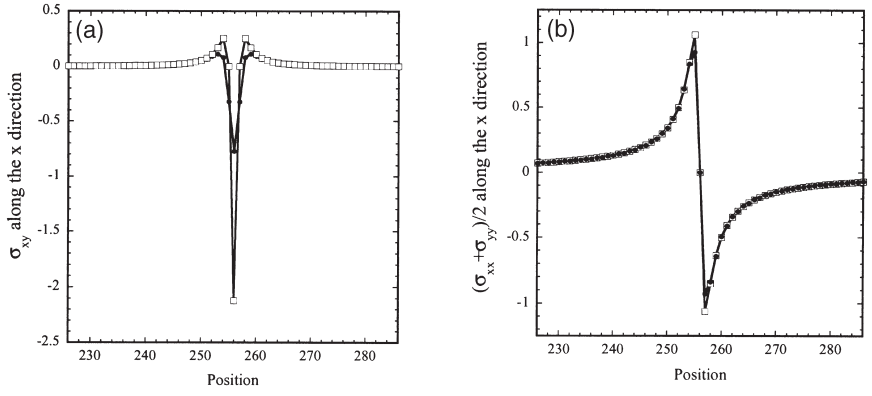

Fig. 4. (a) Shear stress (σ_{xy}) as a function of position along the horizontal line shown in Fig. 1(a). Filled circles—numerical calculation using the Gaussian description with α_1 and α_2 both equal to 1.0; open squares—analytical solution. (b) The local pressure, the average of σ_{xx} and σ_{yy}, along the same line. Solid circles—numerical calculation using the Gaussian description with α_1 and α_2 both equal to 1.0; open squares—analytical solution.

Let us assume that the elastic modulus of the solid solution is isotropic. Following Eshelby [30], the elastic energy density of an elastically isotropic homogeneous solution in two dimensions is

$$e_{\text{hom}} = \frac{2G}{1-\nu}\epsilon_o^2 X(1-X) \tag{28}$$

where G is the shear modulus and ν is the Poisson ratio. Therefore, the incoherent free energy of the ideal solution is given by

$$f^*_{\text{inc}}(c) = f^*(c) + \frac{e_{\text{hom}}}{N_v k_B T} \tag{29}$$

For an ideal solution, the gradient energy coefficient is zero. We performed a numerical simulation using a 256×256 grid and an overall average composition of 0.10. We employed equation (25) for describing the dislocation eigenstrain using $\alpha_1 = \alpha_2 = 1.0$. The dislocation is located at the center, i.e. $x_o = 128.0$, $y_o = 128.0$ and the dislocation direction is along the normal to the 2D domain. We assumed that the composition expansion coefficient was positive with an expansion coefficient of 0.05. The Burgers vector, **b**, is chosen to be (0.0,0.1) in units of Δx. The elastic constants are chosen to make the system elastically isotropic with G (the shear modulus) and ν (the Poisson ratio) equal to 100 and 0.25, respectively. It should be noted that there is no need to assume isotropic elasticity in our numerical calculation and the units for the elastic constants are dimensionless as discussed in the previous section. We solved the diffusion equation with periodic boundary conditions using the semi-implicit Fourier spectral method [29]. The time step for integration is rather arbitrarily chosen to be small, 0.005, for the initial 1000 time steps to maintain the stability for the numerical integration, and then it is increased to 0.5 thereafter. For this substitutional ideal solid solution, an equilibrium segregation profile along a horizontal line just one grid below (see Fig. 1) from the dislocation is shown in Fig. 5 labeled as "numerical simulation". As expected, solutes segregated to the tensile side of the dislocation and depleted at the compressive side. For an isolated dislocation in an elastically isotropic 2D media, the equilibrium segregation profile is analytically described by

$$\ln\frac{X(x,y)}{1-X(x,y)} = -\frac{\epsilon_o G b x}{N_v k_B T \pi (1-\nu)(x^2+y^2)} \tag{30}$$

where x and y are the distances measured from the dislocation along the x and y directions. Using the same values for the modulus, the composition expansion coefficient, and the Burgers vector as in the numerical calculation, the compositional profile

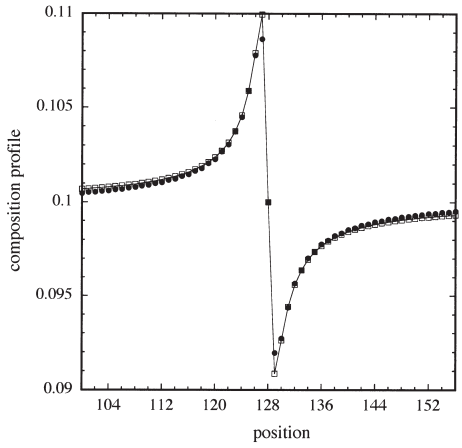

Fig. 5. The equilibrium composition profile around the dislocation for an ideal substitutional solid solution obtained from a numerical calculation using Gaussian description and from an analytical solution.

described by equation (30) is also plotted in Fig. 5 labelled as "analytical solution". As one can see that except very close to the dislocation, the agreement between the analytical solution and the numerical calculation is excellent. The difference is mainly from the different descriptions of the dislocation and boundary conditions. In the analytical solution, the dislocation is described by a singular δ-function in an infinite media while in our numerical calculation it is described by a Gaussian distribution using equation (25) in a periodic media.

To examine a more realistic solid solution, we consider a non-ideal solution. We use the following local coherent free energy density at a given temperature,

$$f^*(X) = (X-0.5)^2[-1.0 + 2.5(X-0.5)^2] \tag{31}$$

It is a double-well free energy function as a function of composition (Fig. 6). The equilibrium compo-

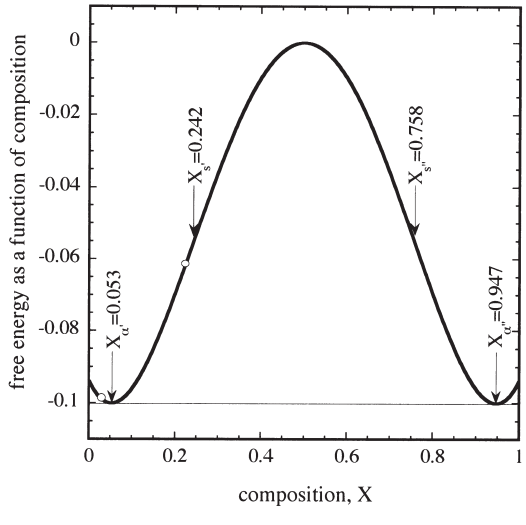

Fig. 6. The coherent chemical free energy as a function of composition.

sitions, $X_{\alpha'}$ and $X_{\alpha''}$, are 0.053 and 0.947, respectively. The spinodal compositions, $X_{s'}$ and $X_{s''}$ are 0.242 and 0.758. As in the case for the ideal solution, the corresponding incoherent free energy, $f^*_{\text{inc}}(X)$ is given by $f^*(X) + e_{\text{hom}}$. We used the same system size and dislocation configuration as in the example for the ideal solution. The initial composition is uniform everywhere with a value of 0.03 which is outside the coherent two-phase field (see Fig. 6). We used the same values for the elastic constants, the composition expansion coefficient, the Burgers vector, and size of time steps as in the ideal solution case. The gradient coefficient is 1.0. In this case, the time step size is 0.05 for the initial 1000 time steps and then it is increased to 5.0 (the semi-implicit spectral method allows a larger time step size with the gradient energy contribution). An example of temporal evolution of the composition profile is shown in Fig. 7(a). The compositions near the dislocation reach their equilibrium values very quickly from an initially homogeneous solution. The solute atoms simply diffuse from the compressive side to the tensile side of the dislocation. The final equilibrium segregation profile is shown in Fig. 7(b).

4.3. Coherent precipitation near an edge dislocation

To examine the nucleation and growth of a coherent precipitate near a dislocation, we use the same free energy model [equation (31)] as in the solute segregation example discussed above. We chose an average composition of 0.22 which is inside the coherent two-phase field, but outside the coherent spinodal region (see Fig. 6). Therefore, in the absence of dislocations, nucleation can occur only when there are fluctuations introduced into the diffusion equation. Indeed, our simulation showed that a solid solution remains homogeneous without the presence of dislocations and thermal noise. When we introduced the same dislocation configuration as discussed in the last section for segregation, it is shown that the homogeneous solution becomes unstable with respect to the nucleation of a coherent particle, i.e. nucleation does not require the presence of thermal noise. We used the same parameters for the elastic modulus, composition expansion coefficient, Burgers vector and gradient energy coefficient as in the solute segregation case. Temporal evolution from a homogeneous solution to nucleation and growth of a precipitate is shown in Fig. 8. It started with segregation of solutes to the tensile side of the dislocation and depletion of solutes on the compressive side. A particle with a composition close to the equilibrium composition of the precipitate phase started to form around $t^* = 5.0$. The nucleus grew by solute diffusion through the matrix. The composition profile around the precipitate presented in Fig. 8(f) is shown in Fig. 9. It can be seen from Fig. 8 that the presence of dislocation also affects the precipitate shapes since, for a system with isotropic elastic modulus and isotropic interfacial energy, the precipitate shape should be spherical or circular in 2D.

The effect of dislocation on the precipitate shape depends on the lattice parameter variation with composition. For example, if the composition expansion coefficient is changed to five times smaller with all other parameters kept the same, the precipitate shape is very close to a circle, i.e. there is no significant effect of dislocation on the precipitate shape [Fig. 10(b)]. With a smaller composition expansion coefficient, the rate of solute segregation is also reduced, and hence it takes a longer time for coherent particles to nucleate.

The precipitate shape also depends on the elastic anisotropy. Figure 10(c) shows a precipitate nucleated around a dislocation in a cubically anisotropic system with overall composition 0.22. In this case, the shape is close to being a rectangle. The elastic constants used in the calculation are $C_{11} = 250$, $C_{12} = 150$, and $C_{44} = 125$ in units of $N_v k_B T$ with all other parameters including the coherent chemical free energy the same as in the elastically isotropic case. This set of elastic constants provides a negative anisotropy with an anisotropic factor of $A = [(2C_{44})/(C_{11} - C_{12})] = 2.5$ and a bulk shear modulus of $\mu = 95$. Without the presence of the dislocation, the precipi-

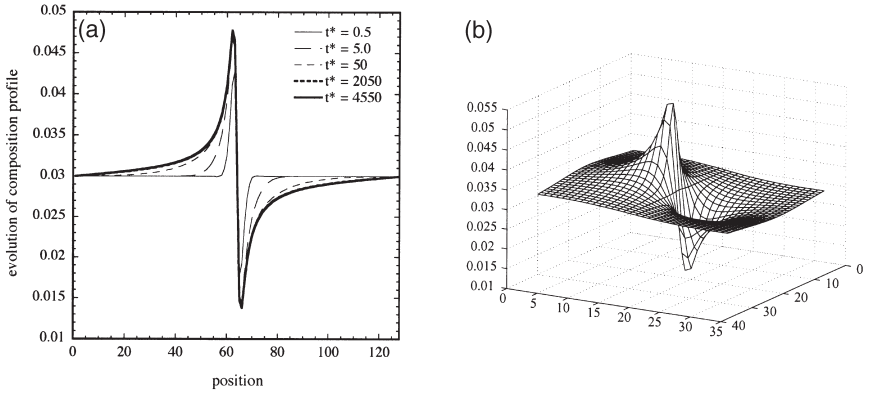

Fig. 7. (a) Temporal evolution of the composition profiles along the horizontal direction one grid point below the dislocation; (b) the equilibrium composition profile around the dislocation.

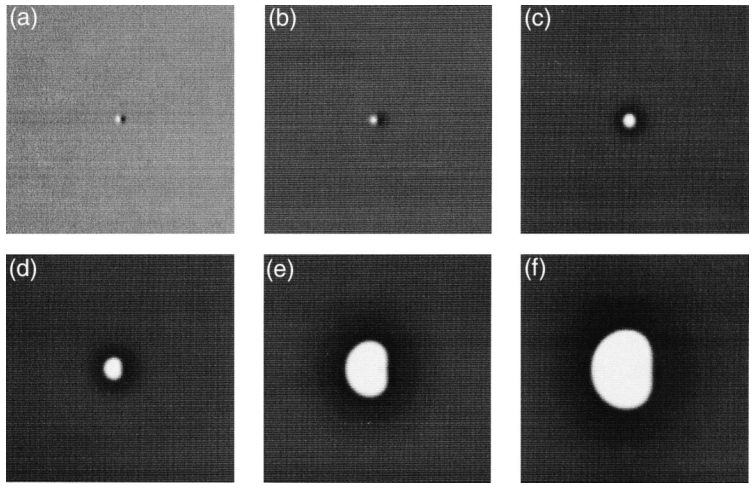

Fig. 8. Morphological evolution during nucleation, and growth of a precipitate near an edge dislocation. (a) $t^* = 0.5$; (b) $t^* = 10$; (c) $t^* = 25$; (d) $t^* = 50$; (e) $t^* = 2050$; (f) $t^* = 4550$.

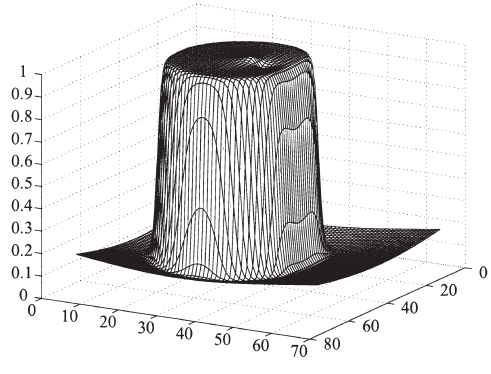

Fig. 9. The composition profile describing the coherent precipitate in Fig. 8(f).

The interaction energy density between a compositional inhomogeneity and a defect field is given by

$$e_{\text{int}} = \sigma_{ij}^{\text{o}}\overline{\delta X(\mathbf{r})\epsilon_{ij}^{\text{d}}(\mathbf{r})} - \int_g \frac{\text{d}^3\mathbf{g}}{(2\pi)^3} n_i \sigma_{ij}^{\text{o}} \Omega_{jk}(\mathbf{n}) \{\sigma_{kl}^{\text{d}}\}_{\mathbf{g}} n_l \, \delta X^*(\mathbf{g}) \tag{33}$$

For a dislocation described by the singular delta function and an elastically isotropic solid solution, the interaction energy between a compositional field and the dislocation field is simplified to

$$e_{\text{int}} = -\frac{\epsilon_{\text{o}}(1+\nu)Gb}{\rho\pi(1-\nu)rk_{\text{B}}T}(X(\mathbf{r}) - X_{\text{o}}) \tag{34}$$

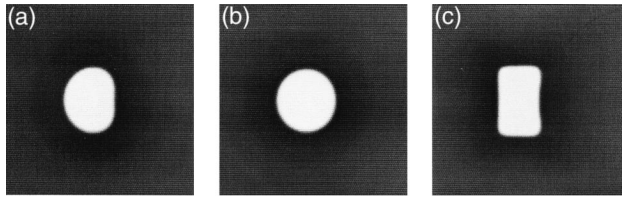

Fig. 10. (a) Precipitate morphology in an elastically isotropic media; (b) precipitate morphology in an elastically isotropic media but with five times smaller composition expansion coefficient than in (a); (c) precipitate morphology in a cubically anisotropic media.

tate shape would be a square with round corners. Therefore, the presence of the dislocation not only leads to the continuous nucleation of a coherent particle but also significantly changes the particle shape.

The barrierless nucleation of a coherent particle around a dislocation can be understood from the elastic coupling between a nucleus and the dislocation. For an isotropic solid solution, the coherency strain energy density is given by

$$e_{\text{coh}} = 2G\frac{1+\nu}{1-\nu}\epsilon_{\text{o}}^2[X(\mathbf{r}) - X_{\text{o}}]^2 \tag{32}$$

From equations (32) and (34), it is easy to see that the coherency strain energy density is proportional to the square of the composition and the interaction energy density is linearly proportional to composition. Therefore, while the coherency strain energy due to a compositional inhomogeneity depresses the spinodal temperature, the introduction of a dislocation field does not affect the position of the spinodal line. Interaction between dislocations and composition simply creates a local potential inhomogeneity which in turn produces a stable compositional fluctuation

(the segregation profile). The critical fluctuations which lead to coherent nucleation can, in principle, be obtained using the non-classical nucleation theory of Cahn [31]. According to Cahn, the energy barrier for coherent nucleation becomes zero when the overall composition approaches the coherent spinodal. In the presence of dislocations, although the overall composition may be outside the coherent spinodal, the local composition may be inside the spinodal as a result of the composition inhomogeneity caused by the dislocation. In our case, since the overall average composition is near the spinodal line, the composition in the tensile side of the dislocation is increased to such an extent that it falls inside the spinodal. As a result, although the overall composition is outside spinodal, the maximum composition around the dislocation already exceeds the spinodal composition and thus produces a compositional instability. Therefore, nucleation and growth in this case can take place without overcoming a nucleation barrier. Indeed, if we choose a composition which is far away from the spinodal composition and perform the simulation without thermal noise, nucleation and growth did not occur. In a real system, the compositional variation from thermal noise is superimposed on the dislocation-induced compositional inhomogeneity, resulting in a variation of nucleation rate with spatial coordinates. Although far away from the spinodal composition, nucleation cannot take place spontaneously in a simulation without introducing thermal noise, it requires a smaller fluctuation to overcome the nucleation barrier, and thus results in an increase in the nucleation rate in the presence of dislocations.

5. SUMMARY

A diffuse-interface field model is proposed for predicting the morphological and microstructural evolution in coherent systems with arbitrary spatial distribution of structural defects such as dislocations. Within this model, the elastic stresses due to a compositional inhomogeneity and structural defects are solved consistently within the same formulation. We also proposed a number of ways to introduce the eigenstrain of a dislocation in practical numerical simulations. We applied our model to solute segregation as well as to the nucleation and diffusional growth of a coherent precipitate at an edge dislocation. It is shown that the coherent nucleation may become barrierless under the influence of the local elastic field of the dislocation even in an elastically isotropic system.

Acknowledgements—The authors are grateful for the financial support from the NSF under the grant No. DMR-96-33719. The simulations were performed at the San Diego Supercomputer Center and the Pittsburgh Supercomputing Center.

REFERENCES

1. Khachaturyan, A. G., *Theory of Structural Transformations in Solids*. John-Wiley and Sons, New York, 1983.
2. Mura, T., *Micromechanics in Solids*. Kluwer Academic Publishers, Dordtrecht, 1982.
3. Larche, F. C. and Cahn, J. W., *Acta metall.*, 1985, **33**, 331.
4. Nishimori, H. and Onuki, A., *Phys. Rev. B*, 1990, **42**, 980.
5. Chen, L. Q., Wang, Y. Z. and Khachaturyan, A. G., *Phil. Mag. Lett.*, 1991, **64**, 241.
6. Wang, Y., Chen, L. Q. and Khachaturyan, A. G., *Acta metall. mater.*, 1995, **41**, 279.
7. Abinandanan, T. A. and Johnson, W. C., *Acta metall. mater.*, 1993, **41**, 17.
8. Thompson, M. E., Su, C. S. and Voorhees, P. W., *Acta metall. mater.*, 1994, **42**, 2107.
9. Sagui, C., Somoza, A. M. and Desai, R., *Phys. Rev. E*, 1994, **50**, 4865.
10. Fratzl, P. and Penrose, O., *Acta metall. mater.*, 1995, **43**, 2921.
11. Koyama, T., Miyazaki, T. and Mebed, A. E., *Metall. Mater. Trans. A*, 1995, **26**, 2617.
12. Lee, J. K., *Metall. Mater. Trans. A*, 1995, **27**, 1449.
13. Jou, H. J., Leo, P. H. and Lowengrub, J. S., *J. Comput. Phys.*, 1997, **131**, 109.
14. Fratzl, P., Penrose, O. and Lebowitz, J. L., *J. Stat. Phys.*, 1999, **95**, 1429.
15. Cottrell, A. H., in *Report of a Conference on Stength of Solids*, ed. N. F. Mott. The Physical Society, London, 1948, p. 30.
16. Cahn, J. W., *Acta metall.*, 1957, **5**, 169.
17. Dollins, C. C., *Acta metall.*, 1970, **18**, 1209.
18. Barnett, D. M., *Scripta metall.*, 1971, **5**, 261.
19. Xiao, S. Q. and Hassen, P., *Scripta metall.*, 1989, **23**, 365.
20. Boulbitch, A. A. and Toledano, P., *Phys. Rev. Lett.*, 1998, **81**, 838.
21. Wang, Y., Srolovitz, D. J., Rickman, J. M. and Lesar, R., *Acta mater.*, 2000, **48**, 2163.
22. Lee, J. K., *Metall. Mater. Trans. A*, 1998, **29**, 2039.
23. Voorhees, P.W., to be published, 1999.
24. Léonard, F. and Desai, R., *Phys. Rev. B*, 1998, **58**, 8277.
25. Cahn, J. W., *Acta metall.*, 1961, **9**, 795.
26. Indenbom, V. L. and Lothe, J., *Book title?*. Elsevier Science Publisher, Amsterdam, 1992.
27. Cahn, J. W. and Hilliard, J. E., *J. Chem. Phys.*, 1958, **28**, 258.
28. Larche, F. C. and Cahn, J. W., *Acta metall.*, 1982, **30**, 1835.
29. Chen, L. Q. and Shen, J., *Comput. Phys. Comm.*, 1998, **108**, 147.
30. Eshelby, J. D., *Solid State Phys.*, 1956, **3**, 79.
31. Cahn, J. W., *Acta metall.*, 1962, **10**, 107.